Contents lists available at ScienceDirect

## Journal of the Mechanical Behavior of Biomedical Materials

Journal of ne Management of old manifest Materials

journal homepage: www.elsevier.com/locate/jmbbm

## Research paper



## Fracture behavior of human cortical bone with high glycation content under dynamic loading

Ebrahim Maghami, Amirreza Sadighi, Ahmad R. Najafi\*

Department of Mechanical Engineering and Mechanics, Drexel University, Philadelphia, PA 19104, USA

#### ARTICLE INFO

# Keywords: Dynamic fracture Cortical bone

Glycation Critical energy release rate Phase field fracture

#### ABSTRACT

The present study simulates the fracture behavior of diabetic cortical bone with high levels of advanced glycation end-products (AGEs) under dynamic loading. We consider that the increased AGEs in diabetic cortical bone degrade the materials heterogeneity of cortical bone through a reduction in critical energy release rates of the microstructural features. To simulate the initiation and propagation of cracks, we implement a phase field fracture framework on 2D models of human tibia cortical microstructure. The simulations show that the mismatch between the fracture properties (e.g., critical energy release rate) of osteons and interstitial tissue due to high AGEs contents can change crack growth trajectories. The results show crack branching in the cortical microstructure under dynamic loading is affected by the mismatches related to AGEs. In addition, we observe cortical features such as osteons and cement lines can prevent multiple cracking under dynamic loading even with changing the mismatches due to high AGEs. Furthermore, under dynamic loading, some toughening mechanisms can be activated and deactivated with different AGEs contents. In conclusion, the current findings present that the combination of the loading type and materials heterogeneity of microstructural features can change the fracture response of diabetic cortical bone and its fragility.

## 1. Introduction

Bone has a hierarchical structure of collagenous protein and minerals in multiple length scales that can activate various toughening mechanisms under normal conditions (Rho et al., 1998). In impact incidents such as car collisions or sports accidents, bone experiences different loading regimes (Hansen et al., 2008). Studies on the mechanical behavior of bone showed that the mechanical properties (e.g., elastic modulus and yielding stress) of bone are influenced by a change in the rate of dynamic loading (Hansen et al., 2008; Zioupos et al., 2008). In addition, the fracture behavior of bone is also found to be rate-sensitive (Zimmermann et al., 2014; Shannahan et al., 2015). In particular, with an increase in the loading rate, the fracture toughness of bone is decreased, and the brittleness of bone is increased (Kulin et al., 2011; Kirchner, 2006).

The risk of bone-related fracture under high loading rates increases with aging and diabetes. One of the changes in bone tissue with diabetes is advanced glycation end-products (AGEs) due to non-enzymatic glycation that accumulates in bone (Vashishth, 2009). AGEs concentrations vary among cancellous and cortical bone as well as different ages (Karim et al., 2019). With all the variations in the reported AGEs concentrations, it is broadly observed that the accumulation of AGEs in bone tissue elevates with aging (Karim and Bouxsein, 2016). As AGEs

accumulate, the mechanical properties and fracture behavior of bone tissue are subjected to changes (Collier et al., 2018). For instance, a high level of AGEs can lead to a decrease in the fracture toughness of human cortical bone (Merlo et al., 2020). In addition, the loss in the dissipation energy during fracture and a more brittle state of diabetic bone are associated with the high level of AGEs (Nyman et al., 2007; Tang et al., 2009; Nyman, 2013). Microdamage accumulation is also found in the bone microstructure with a high AGEs content (Saito et al., 2008; Tang and Vashishth, 2010).

Despite various research on the effect of AGEs on bone tissue, there has not been sufficient in-depth and detailed information yet on how the microstructure of human bone with a high level of AGEs responds to impact events such as accidents or falls where the dominant loading condition is dynamic. To study such mechanisms at the microscale level, a computational approach can facilitate the evaluation of every single parameter that affects the fracture process of bone with high AGEs levels. This is unlike experiments where all uncertainties and variations are included in the evaluation. In this context, there are computational studies that investigated the fracture response of healthy bone under dynamic loading. For instance, dynamic fracture in trabecular bone was simulated by a cohesive finite element method, and it was observed that the microstructural features strongly impact the fracture

E-mail address: arn55@drexel.edu (A.R. Najafi).

https://doi.org/10.1016/j.jmbbm.2024.106577

Received 22 December 2023; Received in revised form 29 February 2024; Accepted 8 May 2024 Available online 11 May 2024

<sup>\*</sup> Corresponding author.

properties under dynamic loading (Tomar, 2008). Another study also used a cohesive finite element model to investigate the influence of various dynamic loading rates on the initiation and propagation fracture toughness of cortical bone (Ural et al., 2011). It is found that toughening mechanisms in bone can be diminished during high-strain loading conditions.

In the current study, we investigate the fracture behavior of cortical bone under dynamic loading. To the best of the authors' knowledge, very few studies, if any, have considered the impact of high levels of accumulated AGEs on the toughening mechanisms occurring in the microstructure of the cortical bone under high strain-rate loadings. Based on the previous studies, an increase in AGEs level can cause a drop in the magnitude of the material properties of bone and bone fragility by decreasing the global fracture toughness (Nyman et al., 2007; Tang et al., 2009; Nyman, 2013). To simulate crack growth trajectories, we implement a phase field fracture method with a brittle framework. In this presented method, cracks are modeled by a diffuse zone and an energy degradation formulation is used to model damage (Miehe et al., 2010). This approach has relatively less numerical instability compared to XFEM and continuum damage mechanics (Wu et al., 2018). In contrast to continuum damage mechanics, damage zone in the phase field method has a thickness, which can be controlled by a length scale parameter (de Borst and Verhoosel, 2016). In contrast to XFEM, the phase field approach overcomes difficulties for crack surface propagation in the presence of multiple cracks nucleation and branching fronts (Nguyen et al., 2015). This diffuse method has been employed to analyze fracture behavior of different materials such as human bone and dentin (Maghami et al., 2022; Josephson et al., 2022; Maghami et al., 2021a,b; Nguyen et al., 2017), brittle biomaterials (Wu et al., 2020), and polymeric nanocomposites (Msekh et al., 2018).

## 2. Materials and methods

#### 2.1. Samples preparation from human cortical bone

A cross-section (50% the mid-shaft length as shown in Fig. 1a) was cut from two cadaveric female human tibias (ages: 60 and 81 as shown in Fig. 1a) collected from a donor bank (Anatomy Gifts Registry, Hanover, MD). We used a silver-nitrate staining method on 8  $\mu m$  thick sections from the samples to more clearly visualize microstructural features such as cement lines at each cross-section (Fig. 1b). We refer the readers for details on the sample preparation and staining method to the previous works (Pinto and Pace, 2015; Josephson et al., 2022; Maghami et al., 2021a). Next, we provide microscopy images from the anterior and posterior regions of the 60-year-old and 81-year-old samples (Fig. 1c). Using a random algorithm, we select three different areas with 1  $mm^2$  in all anterior and posterior samples.

#### 2.1.1. Constructing 2D finite element models

To create the two-dimensional (2D) models, we utilize the microscopy images. To find the boundaries of osteons and Haversian canals, we segment the images with a manual approach. After importing the geometrical data to Abaqus, we build the 2D models (Fig. 1d). The cement lines in our models have a thickness of 5  $\mu m$ . We also consider the homogenized tissue with a thickness of 0.05 mm around the region of the bone sample to avoid any boundary condition effects. Therefore, the dimensions of the models are 1.1 mm by 1.1 mm. All models contain a precrack with 0.05 mm length (Fig. 1e). All of the finite element analyses in this study have been conducted using the "Dynamic, Implicit" solver in Abaqus, where instantaneous load variation with time has been selected in the settings of the solver.

**Table 1** Mechanical properties of cortical features for the 60-year-old samples: critical energy release rate ( $G_c$ ), Young's modulus (E), Poisson's ratio (v), and density ( $\rho$ ) for osteons, interstitial tissue, cement lines, and homogenized tissue.

Material property	Osteon	Interstitial tissue	Cement lines	Homogenized tissue
$G_c$ (N/mm)	$0.62^{b}$	0.52 <sup>b</sup>	0.1629 <sup>b</sup>	0.57 <sup>b</sup>
E (GPa)	16.6a	19.7 <sup>a</sup>	12.45 <sup>d</sup>	18.15 <sup>e</sup>
v	$0.25^{c}$	0.25 <sup>c</sup>	0.3 <sup>e</sup>	0.25 <sup>c</sup>
$\rho$ (g/cm <sup>3</sup> )	$1.62^{f}$	$1.72^{f}$	0.86 <sup>f</sup>	1.68 <sup>f</sup>

- <sup>a</sup> Fan et al. (2002).
- b Brown et al. (2000).
- c Mischinski and Ural (2013).
- d Abdel-Wahab et al. (2012), Budyn et al. (2008), Li et al. (2014).
- e Giner et al. (2017)
- f Gauthier et al. (2019).

## 2.1.2. Mechanical properties of microstructural features

Table 1 represents the mechanical properties of the 60-year-old samples. Using the reported data by Fan et al. (2002), elastic moduli of osteons and interstitial tissue are the average values of the data in the radial direction. We assume  $G_c$  of osteons and interstitial tissue are inversely proportional to the variations in the elastic moduli. This assumption was made based on the information that calcified tissues (e.g., bone) with a high toughness have a lower stiffness (Fratzl et al., 2004). The elastic modulous of cement lines is also calculated as 25% less than the elastic modulus of osteons. An average value from investigations by Giner et al. (2017) is used for  $G_c$  of the cement lines. In addition, the average values of osteons and interstitial tissue are calculated for the mechanical properties of the homogenized region in all models. The material properties of all individual features are considered to be homogeneous and isotropic. With the properties in Table 1 as the base data for the 60-year-old models, we calculate the material properties of the 81-year-old samples using the function between age and the material properties reported by Brown et al. (2000).

#### 2.2. The relationships between AGEs and $G_c$

In human cortical bone, AGEs content can increase with age and there is a relationship between a decrease in the energy release rate  $(G_c)$  and the elevated concentration of AGEs (Tang and Vashishth, 2011). Aligned with these observations and studies (Tang and Vashishth, 2011; Jia et al., 2021; Campbell et al., 2016), a reduction in  $G_c$  of osteons, interstitial tissue, and cement lines has been taken into consideration with the increased AGEs in the 60-year-old and the 81year-old samples. Furthermore, even though a number of studies have been conducted to investigate the adverse impact of increased AGEs on the mechanical and fracture properties of bone microstructural features, the magnitude of the reduction is still uncertain. Therefore, in order to check how the fracture response of bone is affected by variations in the fracture properties of these microstructural features, three possible scenarios have been considered for the mismatch ratios  $(R_G)$  between  $G_c$  of osteons and interstitial tissue, which is defined as  $R_G = \frac{G_{ost} - G_{int}}{G_{ost}} \times 100\%$ , as depicted in Table 2.

## 2.3. Computational simulation sets

Like mentioned in Section 1, the objective of the study is to look into the fracture response of cortical bone with elevated levels of AGEs under dynamic loading at the microstructural level. More specifically, we are curious to know, given the same dynamic loading case, how further accumulation of AGEs with age and diabetes is going to impact the fracture response, what scenarios might happen with this increase, and how this fracture response and associated toughening mechanisms differ from the case of very low strain rate (findings of previous research where quasi-static condition was considered (Maghami et al., 2021a)). In doing so, the following sets of simulations are to be conducted:

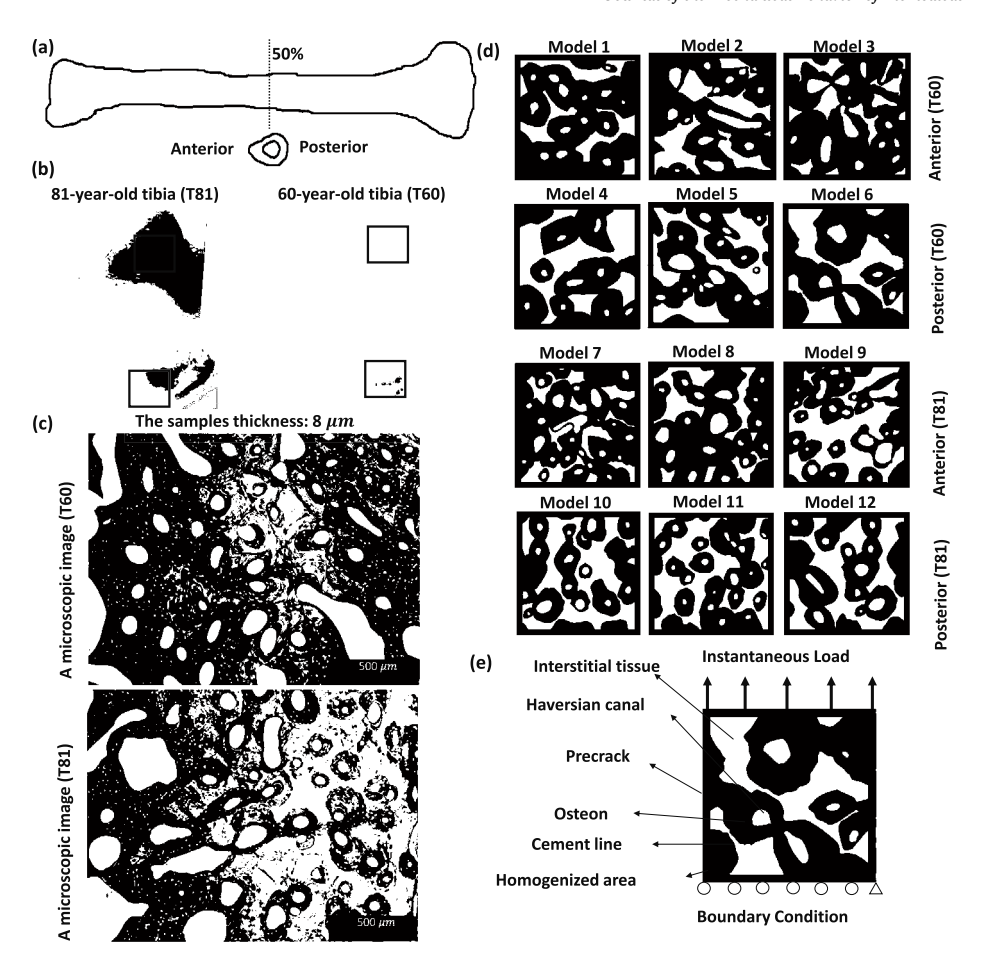


Fig. 1. (a) The schematic of human tibia and the 50% cross-section, (b) the thin cross-sections from the samples with 81 and 60 ages, (c) two microscopy images taken from the samples after the staining technique, (d) the 2D created models, and (e) the loading boundary conditions on all models.

Table 2 Three possible values for the mismatch between  $G_{ost}$  and  $G_{int}$  at the level of 100% increase in AGEs.  $R_G$  indicates the mismatch ratio in each case.

Loss in critical energy release rates of osteons and interstitial tissue (%)	Mismatch ratio between $G_{ost}$ and $G_{int}$ : $R_G = (\frac{G_{ost} - G_{int}}{G_{ost}}) \times 100\%$
20% loss in $G_{ost}$ and 70% loss in $G_{int}$	$R_G = 75\%$
30% loss in $G_{ost}$ and 60% loss in $G_{int}$	$R_G = 50\%$
45.5% loss in both $G_{ost}$ and $G_{int}$	$R_G = 15\%$

- (i) We simulate the fracture behavior of the anterior and posterior regions of the 81- and 60-year-olds under the same dynamic loading condition. In this set of simulations, the aim is to compare the fracture response of the models from two different ages (81 and 60). Thus, all simulations in this set have the same dynamic loading condition considering an instantaneous loading with a rate of  $10^{-6}$  mm/s.
- (ii) We simulate the fracture behavior of each model presented in Fig. 1d with each case of the mismatch ratio in Table 2 under dynamic loading. Our purpose is to compare crack growth trajectories in each region with another region as well as regions of the two ages. We use the same instantaneous loading condition in the previous set (i).
- (iii) In this set, we randomly compare the fracture response of the models 1, 7, 11, and 12 under dynamic loading with their response under quasi-static loading. Our aim is to understand how fracture behavior changes under dynamic loading and what

toughening mechanisms become activated or deactivated. We apply the same instantaneous loading condition presented in set (i).

## 2.4. A phase field framework for dynamic fracture

In the present study, we utilize a phase field method presented by Miehe et al. (2010) to analyze the dynamic fracture behavior of cortical bone. In this diffusive fracture framework, to model crack growth, the minimization problem of an energy functional of a material takes the form

$$\Pi^{int} = E(\mathbf{u}, d) + W^{dmg}(d), \tag{1}$$

where  $\Pi^{int}$ , E(u,d), and  $W^{dmg}(d)$  are the total potential energy, the elastic energy, the work to form cracks surface, respectively. Damage field variable (d $\in$  [0,1]) introduces the unbroken (d=0) and broken states (d=1) of the material, respectively. u describes the displacement field in the material.

The elastic energy in the cracked material is defined such that

$$E(\mathbf{u}, d) = \int_{\Omega} \Psi(\epsilon(\mathbf{u}), d) d\Omega, \tag{2}$$

where  $\Psi(\varepsilon(u),d)$  is the strain energy density and  $\varepsilon(u)$  is the symmetric strain tensor. We refer the readers to the work of Miehe et al. (2010) for more details on the stress tensor and the degraded strain energy.

 $W^{dmg}(d)$  in Eq. (1) has the form such that

$$W^{dmg}(d) = \int_{\Omega} G_c \, \gamma(d, \nabla d) \, d\Omega, \tag{3}$$

where  $G_c$  is the critical energy release rate and  $\gamma(d,\nabla d)$  is the crack density function forms such that

$$\gamma(d, \nabla d) = \frac{1}{2l_c} d^2 + \frac{l_c}{2} \nabla d \cdot \nabla d, \tag{4}$$

where  $l_c$  is the length scale parameter describes the width of the damaged zone between the unbroken and fully broken states of the material (the crack width) (Bourdin et al., 2008). The diffusive crack in phase field method is presented by the regularized crack surface function.

To find the solution for dynamic fracture, the energy functional of the whole problem  $(\Gamma)$  can be defined

$$\Gamma = D(\dot{u}) - \Pi^{int} + W^{ext} = D(\dot{u}) - E(u, d) - W^{dmg}(d) + W^{ext}, \tag{5}$$

where  $\dot{u}$  is the local velocity. With the mass density of the material  $(\rho)$ ,  $D(\dot{u})$  describes the kinetic energy of the body

$$D(\dot{\mathbf{u}}) = \int_{\Omega} \frac{1}{2} \rho \dot{\mathbf{u}} \dot{\mathbf{u}} d\Omega. \tag{6}$$

The external work  $(W^{ext})$  is defined by body forces  $(\bar{b})$  and boundary tractions  $(\bar{t})$ 

$$W^{ext} = \int_{\Omega} \bar{\mathbf{b}} \cdot \mathbf{u} \, d\Omega + \int_{\partial\Omega} \bar{\mathbf{t}} \cdot \mathbf{u} \, d\partial\Omega. \tag{7}$$

In addition, the energy functional for the displacement field problem is described by

$$\Pi^{u} = \int_{\Omega} (\Psi(\varepsilon(\mathbf{u}), d) + \frac{4\rho}{\tau^{2}} (\frac{|\mathbf{u}|^{2}}{2} - \tilde{\mathbf{u}}_{n}\mathbf{u}) - \bar{\mathbf{b}}.\mathbf{u}) d\Omega - \int_{\partial\Omega} \bar{\mathbf{t}}.\mathbf{u} d\partial\Omega,$$
(8)

where Newmark algorithm has been used to perform the time integration of the displacement field. In doing so, through constant-average acceleration method (or trapezoidal rule),  $\tilde{u}_n = u_n + \ddot{u}_n \tau + \ddot{u}_n \tau^2/4$  is approximated based on the previous time step (n) variables with the time increment of  $\tau$ , where  $\ddot{u}$  is acceleration (Hofacker and Miehe, 2013). The energy functional for the phase field problem defines such that

$$\Pi^{d} = \int_{\Omega} \left( G_{c} \gamma(d, \nabla d) + (1 - d^{2}) \mathcal{H} \right) d\Omega, \tag{9}$$

where  $\mathcal{H}$  denotes strain history functional, which is the connection between the displacement field and phase field and ensures the irreversibility of the damage growth. More details on the strain history functional can be found in the work of Hofacker and Miehe (2012). To find the strong forms for each field (the phase field and displacement), we construct the variations of the two energy functionals presented in Eqs. (9) and (5). The readers can find more detail on deriving the strong forms in the works of Hofacker and Miehe (2012) and Liu et al. (2016).

We solve the phase field and displacement problems using a staggered technique in a user-defined element subroutine (UEL) into Abaqus presented by Molnar et al. (2020). The finite element discretization is established based on the studies conducted by Molnár and Gravouil (2017), Molnar et al. (2020). All 2D models have fournode elements. The number of elements in all models is nearly between  $\sim$ 550,000 and  $\sim$ 600,000. We also carry out mesh convergence tests for all models. As shown in Fig. 1, we apply an instantaneous dynamic force on the top edge of the 2D models. The constraints for the boundary conditions (depicted in Fig. 1) are the fixed bottom edge along the y direction and the fixed bottom left corner along the x and y directions. We also consider the length scale parameter in all simulations to be  $I_c = 0.001$  mm denoting the damaged zone thickness (Eq. (4)). This choice was made to ensure that the crack bandwidth is less than the smallest scale in the FEM.

### 3. Results

In this section, we look into different post-yielding behaviors of cortical bone samples with increased AGEs under dynamic loading. We investigate changes in the total damage accumulation and damage

Table 3

The total damage accumulation and damaged cement lines for each mismatch case  $(R_G)$  of each model. The percentages are compared to the original models in Fig. 2.

		Total damage accumulation (%)			Total damaged cement lines (%)			
	$R_G$	15%	50%	75%	$R_G$	15%	50%	75%
60-year-old models								
1		12	14	19		6	7	50
2		2	3	3.5		7.1	7.15	7.16
3		8	4	3		1.6	1.5	1.4
4		-21	1	1		-10	2	2
5		2	5	6.5		6	8	12
6		10	11.5	13.2		15.4	45.7	63.4
81-year-old models								
7		15	22	31		5	8.5	12.7
8		-8.7	-8.2	0		0	0	0
9		5.4	-6.3	-6.7		5.4	14.2	18.4
10		-4.5	-4.6	-4.5		-2.6	-2.8	-2.9
11		2.5	-37.6	4.2		1.1	-5.2	2
12		5.8	6.3	6.7		0	0	0

cement lines as well as activation or deactivation of toughening mechanisms with increasing mismatch ratio due to elevated AGEs. We also compare the fracture responses of some models under dynamic loading with the same models under quasi-static loading.

Fig. 2 shows the fracture response of the models (the models 1-12 shown in Fig. 1d under the same dynamic loading mentioned in Section 2.3). Here, we compare the dynamic fracture behavior of the models of age (60) with that of the other (81). Crack deflection, crack branching, microcracking, and crack propagation in cement lines occur in our simulations on both the 60- and 81-year-old models (Fig. 2). In addition, many of the cracks initiate from the Haversian canals (Fig. 2). Our simulations also indicate that the Haversian canals attract and deflect the main cracks from their original path due to the high-stress concentration. In some models (such as the models 2 and 5), a large Haversian canal can cause stress concentration and the crack to initiate from. This would not let the crack nucleate in the other Haversian canals in its surrounding (Fig. 2). Additionally, microcracking can initiate in other models around the smaller Haversian canals. On average, the rate of crack propagation in the 60-year-old models is 8.5% higher than that of the 81-year-old models.

Figs. 3 and 4 depict the fracture behavior of the 60-year-old anterior models (the models 1–6) with variations in the bone microstructural fracture properties due the increased AGEs levels and the three consequent mismatch ratios ( $R_G = \frac{G_{ost} - G_{int}}{G_{pst}} \times 100\%$ ) under the same dynamic loading in Section 2.3. The fracture results and changes in damage accumulations of each model for the three cases  $R_G$  have been compared with those depicted in Fig. 2 and reported in the previous paragraphs, and have been displayed in Table 3. Accordingly, a negative sign denotes less damage accumulation.

As an illustration, in the model 1, the crack accumulation increases with an increase in the mismatch ratio (from  $R_G=15\%$  to  $R_G=75\%$ ). In this model, we also observe more damage propagation in cement lines in the highest mismatch ratio case ( $R_G=75\%$ ) as well as the occurrence of the crack branching mechanism in this mismatch case. However, in the model 2, due to the existence of a large Haversian canal, there are negligible differences in crack growth trajectories (total crack accumulation and crack propagation in cement lines) among three mismatch ratios (Fig. 3). In the model 3, the case with the lowest mismatch ratio ( $R_G=15\%$ ) has the highest rate of total damage accumulation and there are no significant differences between the crack propagation in cement lines among the mismatch cases.

The total damage accumulation in the model 4 with the  $R_G=15\%$  case is lower than that of other cases ( $R_G=50\%$  and 75%) (Table 3). The results for this model, as depicted in Table 3, also show damage accumulation in cement lines in the cases with  $R_G=75\%$  and 50% is more than that of the other case ( $R_G=15\%$ ). We also observe

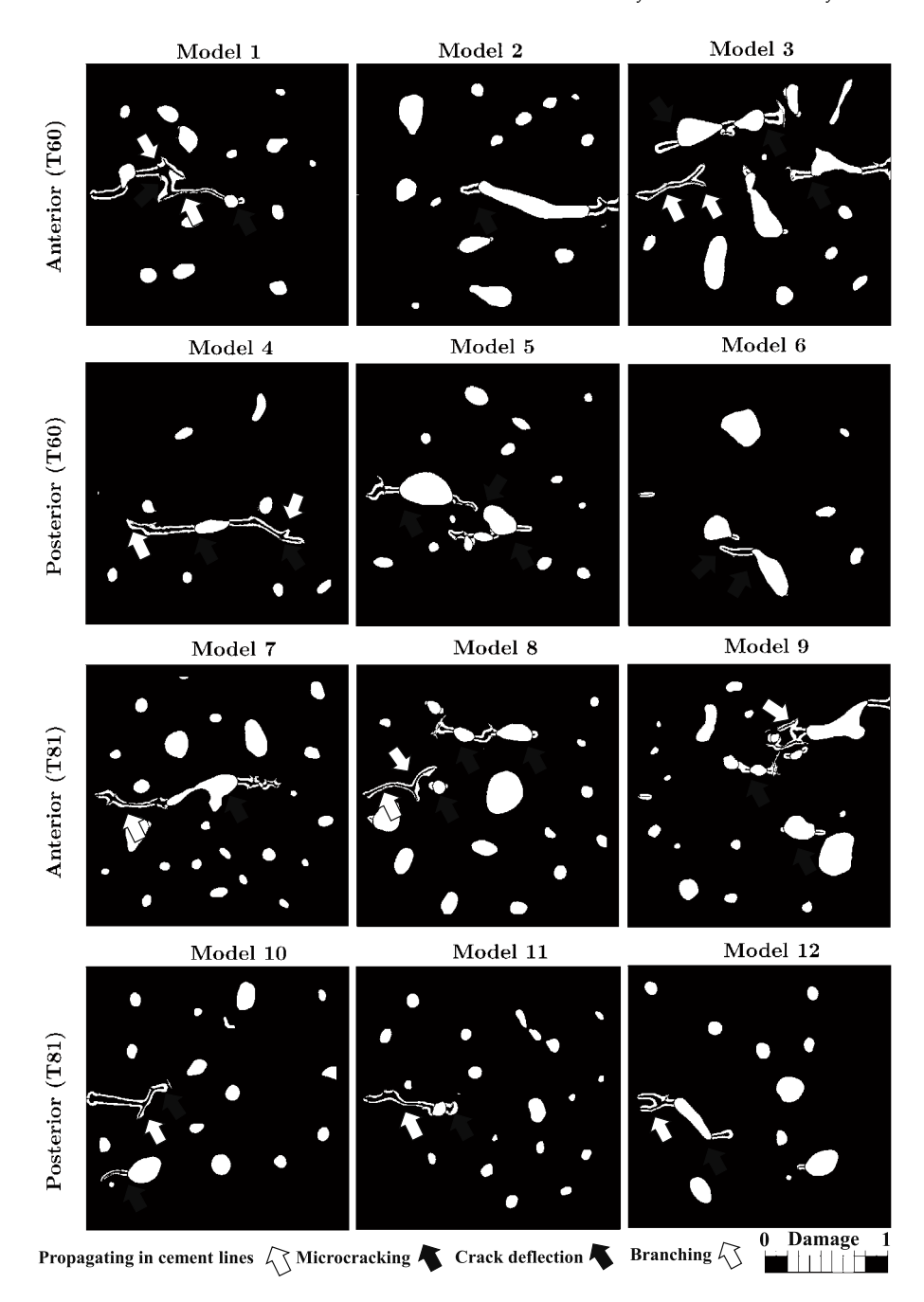


Fig. 2. The dynamic fracture results of the 2D models (Models 1–12) in Fig. 1d under the same instantaneous loading in Section 2.3. Different fracture mechanisms are activated such as crack deflection, microcracking, and crack branching.

more damage accumulation in osteons rather than cement lines in the case  $R_G=15\%$  for the model 4. In the model 5, there are two large Haversian canals in the middle that concentrated the damage accumulation. The damage initiation patterns from the canals in the three mismatch cases in the model 5 are nearly the same. However, in the model 5, the highest mismatch case ( $R_G=75\%$ ) has a higher percentage of damage growth in cement lines (Table 3). Additionally, in the model 6, the rate of crack propagation in cement lines increases with an increase in the mismatch value. The high percentage of damage in the model 6 with the cases  $R_G=50\%$  and  $R_G=15\%$  accumulates in osteons.

Figs. 5 and 6 depict the fracture simulations of the anterior models with age 81 with three different mismatch ratios ( $R_G=15\%$ , 50%, and 75%) under the same dynamic loading in Section 2.3. The fracture patterns of each model with different mismatch ratios are compared

with one another based on the total accumulation of microcracks and damaged cement lines.

To demonstrate, in the model 7, we observe more damaged cement lines in the case with the highest mismatch case ( $R_G=75\%$ ) than that of other cases (Table 3). In addition, in this model, cracks can propagate roughly 20% more in osteons in the case with the lowest mismatch ( $R_G=15\%$ ). However, in the case of model 8, there are no significant differences among all the  $R_G$  cases, except, there are more microcracks around some Haversian canals in the case  $R_G=15\%$ . Furthermore, in the model 9, there is a higher accumulation of damage in the case with the lowest mismatch ratio ( $R_G=15\%$ ) than in the other cases. We further observe more damage propagation in cement lines in the case by increasing the mismatch value (from  $R_G=15\%$  to 75%).

Additionally, changes in  $R_G$  have negligible effects on the crack growth trajectories and the occurrence of the toughening mechanisms

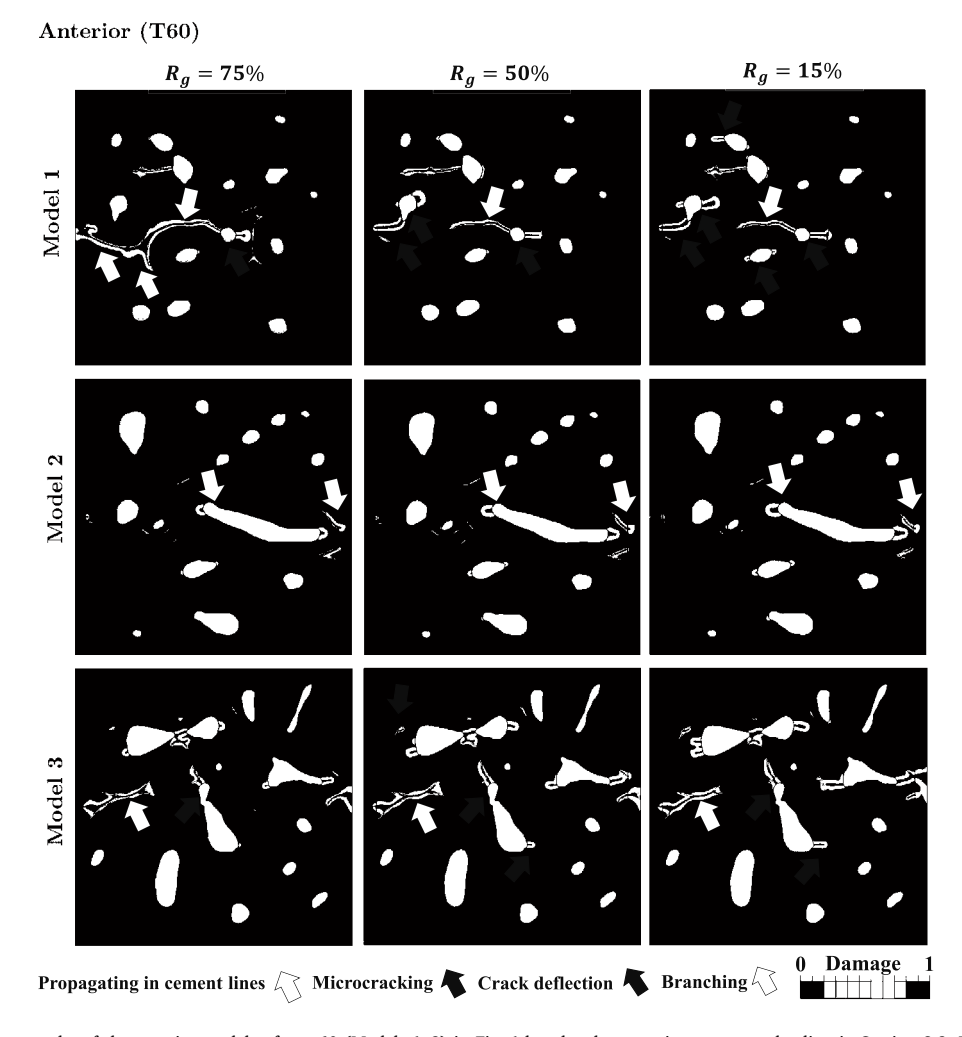


Fig. 3. The dynamic fracture results of the anterior models of age 60 (Models 1–3) in Fig. 1d under the same instantaneous loading in Section 2.3. The fracture results of three  $R_G$  ratios are shown for each model.

in the model 10 (Fig. 6 and Table 3). In this model, for instance, with the case  $R_G=75\%$ , two microcracks occur at one side of the Haversian canal, as shown in Fig. 6, while one microcrack forms on the same side of the canal in the cases of  $R_G=15\%$  and  $R_G=50\%$ . This could lead to crack branching with the advance of load or in case the loading rate increases. In the model 11, the case  $R_G=50\%$  has lower damage accumulation than that of other cases. We also observe crack branching in the  $R_G=75\%$  case in this model whereas other cases in the same model do not include this mechanism. In the model 12, there are negligible differences in crack growth trajectories and the total crack accumulation among the three  $R_G$  cases (Fig. 6 and Table 3).

We further investigate the fracture response of cortical bone under dynamic loading and quasi-static loading. Fig. 7 depicts the fracture responses of the models 1, 7, 11, and 12 under two types of loading, quasi-static and dynamic. This set of simulations shows the differences in crack growth trajectories between the two loading types for each model and reports the changes in toughening mechanisms from the quasi-static to dynamic condition.

In the model 1, damage propagation in cement lines in the dynamic case is 78% higher than that of the quasi-static case. In addition, in this model, we also observe crack branching in the dynamic case. However, in the model 7, as shown in Fig. 7, we observe 58% lower crack propagation in cement lines under dynamic loading than in quasi-static case. Moreover, in this model under dynamic loading, cracks can break the osteons as shown in Fig. 7. Additionally, in the model 11, we observe a 35% rise in crack propagation in cement lines while under

dynamic loading compared to the quasi-static one. There are also more microcrack formations around the Haversian canals in this model under quasi-static loading than under dynamic loading. Moreover, the loading type can change the occurrence of crack branching. For instance, in the model 12, cracks initiate from the Haversian canals and we observe crack branching (the green arrow that shown in Fig. 7). Nevertheless, there is no branching in the quasi-static case in the model 12.

## 4. Discussion

In the present study, we simulate the dynamic fracture behavior of diabetic human cortical samples by utilizing a phase field fracture framework. Our aim is to investigate the influence of changes in the mismatches between the microstructural properties on the fracture behavior of cortical bone with increased AGEs due to diabetes levels under dynamic loading. One benefit that such numerical framework offers is the fact that parameters, such as toughening mechanisms and stress fields in the microstructural scale can be investigated, while such analysis in experiments would either be too costly or infeasible. We simulate fracture in cortical bone by constructing 2D plane strain models from the microscopy images of two human tibias (ages 60 and 81). Our assumption is based on the fact that the longitudinal size in the tibia is relatively higher than its average transverse dimensions. Therefore, it can be concluded the strain in the longitudinal direction is far lower than strains in the transversal direction. In addition to that, the loading condition in our models is in the transverse plane and it does

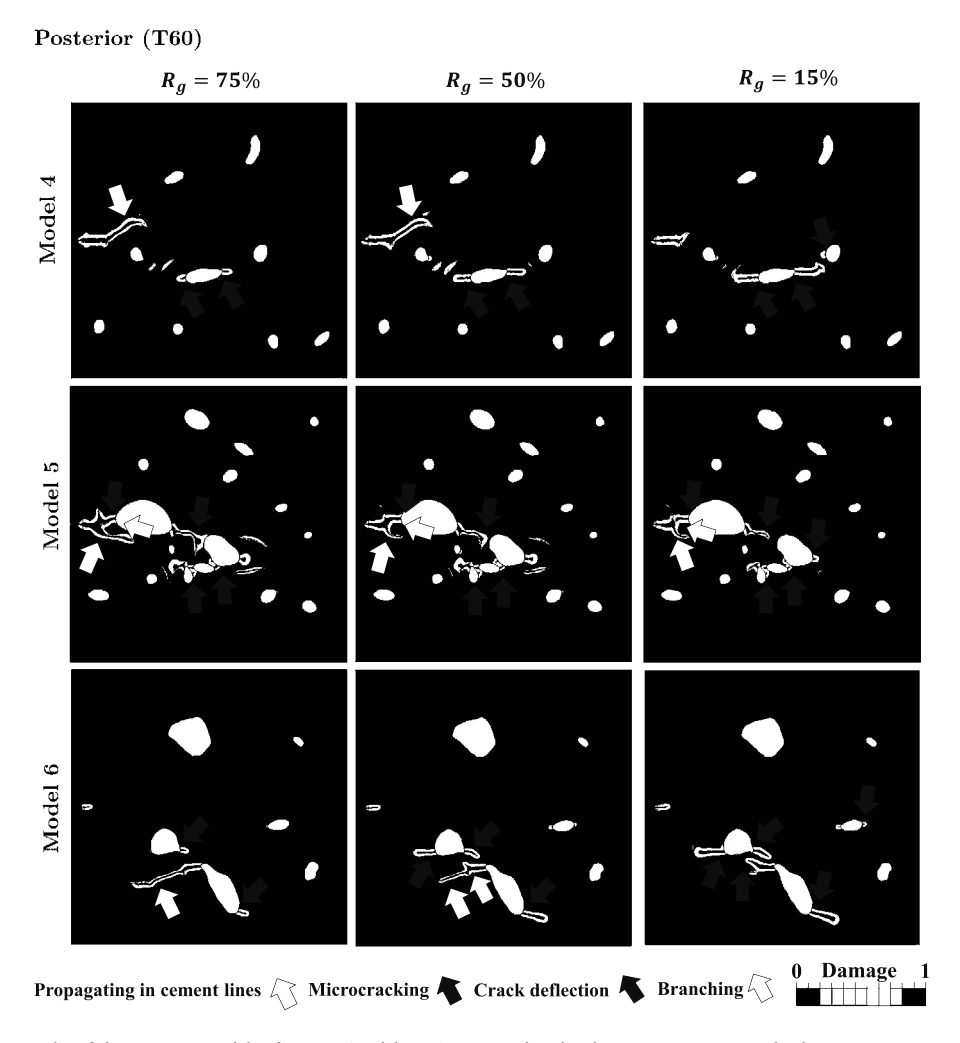


Fig. 4. The dynamic fracture results of the posterior models of age 60 (Models 1–3) in Fig. 1d under the same instantaneous loading in Section 2.3. The fracture results of three  $R_G$  ratios are shown for each model.

not change the length of the whole bone. These are the justifications for the plane strain assumption in our model and it is in agreement with other works (Gustafsson et al., 2019; Saffar et al., 2013; Abdel-Wahab et al., 2012). Accordingly, without eradicating the possibility of the fact that cracks in bone might initiate and propagate initially in the transverse direction and then continue in the longitudinal one, our analysis only focuses on the propagation in the microstructural level in the transverse plane and the changes in the toughening mechanisms due to elevated levels of AGEs. Moreover, the findings and observations of the current study have been compared to those from our previous experimentations (Najafi et al., 2011), and given the similar fracture responses and toughening mechanisms reported, this framework and its findings have been qualitatively validated.

In the literature of cortical bone with diabetes, measuring AGEs level is performed for the whole bone samples and not measuring the AGEs level in each individual microstructural feature of cortical bone (e.g., osteons and interstitial tissue). In the current study, our assumption is that AGEs accumulation can lead to changes in the mismatch between the fracture properties of the microstructural features. This assumption is based on the fact that AGEs accumulation might be affected by bone turnover (Karim and Bouxsein, 2016; Burr, 2019) and the accumulated AGEs level in osteons might be different from that of the interstitial tissue. Therefore, we assume various mismatches between the fracture properties of osteons and interstitial matrix. Here, we define the mismatch ratios such that  $R_G = 15\%$ , 50%, and 75%.

To investigate the influence of such changes in AGEs accumulation on the fracture behavior of cortical bone, we look into the post-yielding behaviors of cortical bone such as the total damage accumulation, the percentage of damaged cement lines, and the occurrence of different toughening mechanisms. The results from the present simulations show that the post-yielding features such as damage accumulation and crack growth trajectories can be influenced by changing the mismatch ratio  $(R_G)$  under dynamic loading. As an example, in the results of some models (1, 5, 6, 7, and 9), we observe more damage accumulation and propagation in cement lines in the case with a high mismatch. However, this trend is not observed for other models.

In addition, crack growth trajectories and the total crack accumulation are unchanged or have minor changes with increasing the mismatch ratio  $(R_G)$  in some of the present simulations. For instance, in the models 8 and 12, there are negligible changes among the mismatches. A possible justification for such minor differences might be that the geometry of osteons and canals are in a way that have the major impact on crack trajectory and toughening mechanisms prevents cracks from propagation under sudden loading. Even if there is still some changes in the materials properties of microstructural features due to alterations in bone turnover related to high levels of AGEs. For example, in the model 12, there is a large Haversian canal that dominates the damage accumulation in its surroundings and changing the mismatch ratios cannot affect the overall crack growth trajectories. We also observe that experimental reports on the influence of AGEs on the post-yielding behavior of cortical bone are not consistent. For instance, it is found that the fracture initiation toughness (as a fracture property) does not differ from control samples to glycated samples in

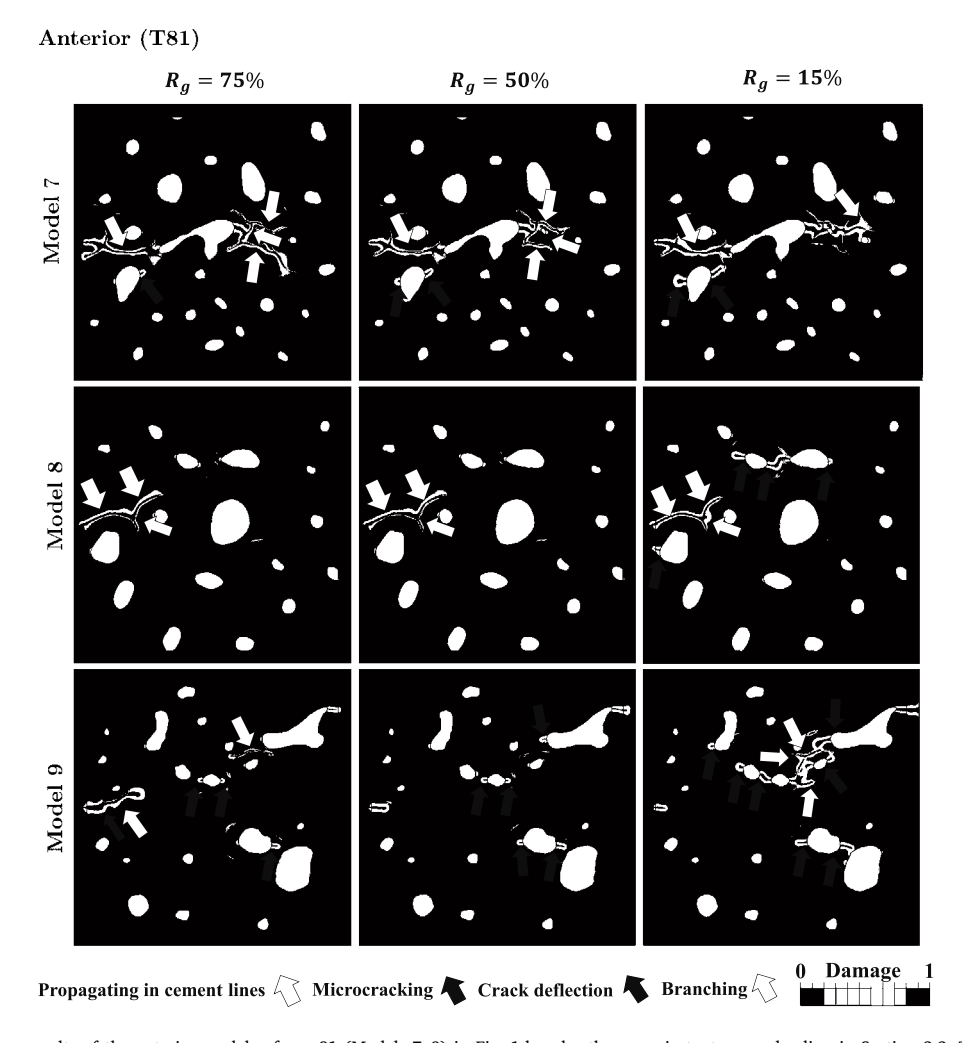


Fig. 5. The dynamic fracture results of the anterior models of age 81 (Models 7–9) in Fig. 1d under the same instantaneous loading in Section 2.3. The fracture results of three  $R_G$  ratios are shown for each model.

cortical bone (Poundarik et al., 2015). However, in another study, it is concluded that the higher the AGEs level is, the lower fracture initiation toughness is displayed by human cortical bone (Merlo et al., 2020). A possible reason for the reported variations in fracture toughness still can be related to differences in the size and formation of the microstructural features (Carando et al., 1989).

In addition to the differences in the geometrical features, an important factor in understanding the fracture behavior of cortical bone is the rate of applied loading (Zimmermann et al., 2014; Shannahan et al., 2015). For instance, the increased loading rate reduces bone fracture toughness and increases the degree of brittleness in bone (Kulin et al., 2011; Kirchner, 2006). Our current simulations also show that crack trajectories in the samples under quasi-static loading differ from that of cases under dynamic loading. In the quasi-static cases, in general, cracks have the chance to propagate over time and multiple toughening mechanisms can be activated. However, in the dynamic cases, due to an instantaneous loading, some of the toughening mechanisms are deactivated. For instance, we observe less crack propagation in cement lines in the dynamic cases and cracks break more osteons or cracks can branch in different directions.

This study investigated the fracture response of the bone with respect to the microstructural features and their fracture properties. Even though the observations and conclusions were made based on the microscale, it is noteworthy that it has already been shown that with age, the variations of mechanical properties between osteonal and interstitial regions within bones become more pronounced (Phelps et al.,

2000). These distinctions can lead to elevated stress concentrations and microcracks, which could ultimately eventuate in the propagation of macroscale cracks along the interface or cement lines and failure of bone. Accordingly, to have a better perspective, the impact of elevated AGEs level and the correlation between the effective initial linear response (stiffness) and the fracture response has been demonstrated in the figure below (Nguyen et al., 2019). Fig. 8a shows the stressstrain curve for the two different ages (Models 1 and 7 representing T60 and T81, respectively) and different mismatch possibilities due to elevated AGEs level, Fig. 8b schematically exhibits how the elastic  $(W_{el})$  and post-yield  $(W_{py})$  energy absorption is calculated from forcedisplacement curves, Fig. 8c displays the force displacement curves for the above-mentioned models, and Fig. 8d compares the impact of increased levels of AGEs on the mechanical response of the bone of different models. As it can be seen, with age and associated changes in the material properties, not only does the effective initial (linear) elastic stiffness of bone decrease and bone become more brittle, but also the capacity of bone to absorb the post-yield (fracture) energy plunges. As an illustration, the effective elastic stiffness and  $W_{py}$  decline by over 53% and 70% from the model  $T61 - R_g = 75\%$  to  $T80 - R_g = 15\%$ , respectively.

Moreover, it is observed the microstructural features, especially cement lines, have an important role in determining the fracture response and the development of bone failure (Abdel-Wahab et al., 2012). Therefore, investigating the possible scenarios for the microstructural property mismatch arising from increasing AGEs level and their impact

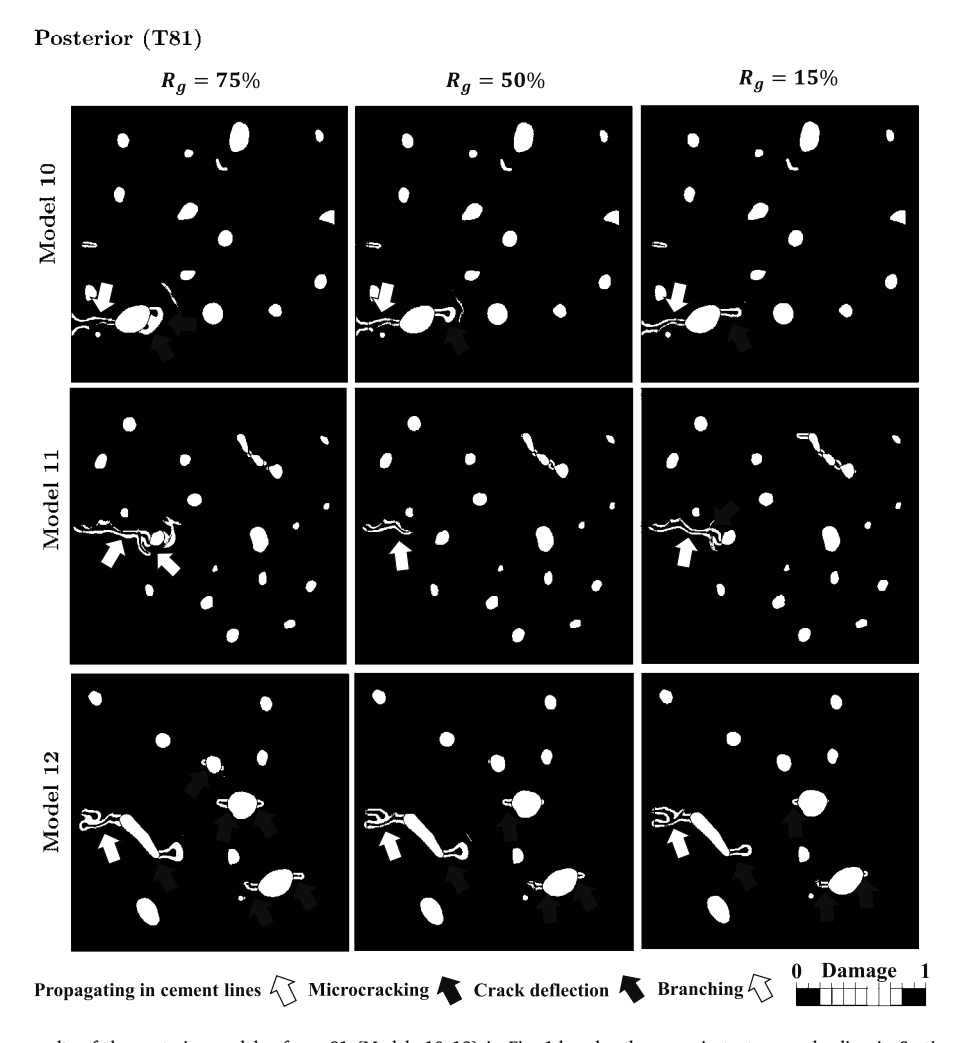


Fig. 6. The dynamic fracture results of the posterior models of age 81 (Models 10–12) in Fig. 1d under the same instantaneous loading in Section 2.3. The fracture results of three  $R_G$  ratios are shown for each model.

on the fracture response of bone microstructure, can provide us with important outlooks regarding the global response of bone and result in the improvement of bone assessment in clinical practice and fracture risk prediction (Augat and Schorlemmer, 2006). This is even more significant in real-life conditions where the dominant loading type is dynamic, about which very little, if any, work had been done.

It should be noted that the simulations in our current study have some limitations. The 2D models cannot define cracks propagation along the longitudinal axis of the long bone. In addition, there are some pre-existing microcracks in the microscopy images of the samples. However, these are not included in our models. We also assume only three mismatch cases between the fracture properties of the microstructural features whereas AGEs can cause more uncertainties (and therefore more scenarios) in those mismatches due to the high variations in the AGEs content at different ages. Furthermore, the length scale parameter  $l_c$ , which in this research was based on a reasonable consideration of geometrical features of the FEMs, in the phase field framework is also suggested to be a material parameter (Mandal et al., 2019) and further investigations are required to find the relationship between  $l_c$ and fracture properties of that material (even though this statement is still under debate (Zhang et al., 2017)). Also, as shown before, this parameter does not impact toughening mechanisms and fracture response of bone, and only scales up/down the force-displacement results and crack bandwidth (Maghami et al., 2021a). Accordingly, the findings and observations in this study are independent from this parameter. As a future study, the dynamic phase-field fracture framework can be

modified to include the cohesive laws to ensure the independence of the results from this parameter (Verhoosel and de Borst, 2013). It is also noteworthy that the microstructural features of cortical bone, i.e. osteons and interstitial tissues, have been modeled as continuum sections with homogenized material properties. This simplification was deemed as considering the actual geometrical features of osteons, which consists of concentric layers, would significantly require higher numbers of elements, causing the analyses to be computationally too expensive and heavy. However, the material properties obtained through homogenization were still able to capture the global response even though some local responses might have been overlooked. Furthermore, as a future study, different scales and dimensions for the microstructure of the cortical bone can be considered in 2D FEMs in order to investigate the boundary and dimensional effects on wave reflections under dynamic loading conditions.

#### 5. Conclusion

The present study investigates the influence of changes in the mismatch between the properties of microstructural features (due to increased AGEs levels) on the dynamic fracture behavior of cortical bone. The presented phase-field fracture framework is a practical numerical tool to simulate various toughening mechanisms and crack growth trajectories under both quasi-static and dynamic loading conditions. In addition, the role of microstructural features on the fracture response

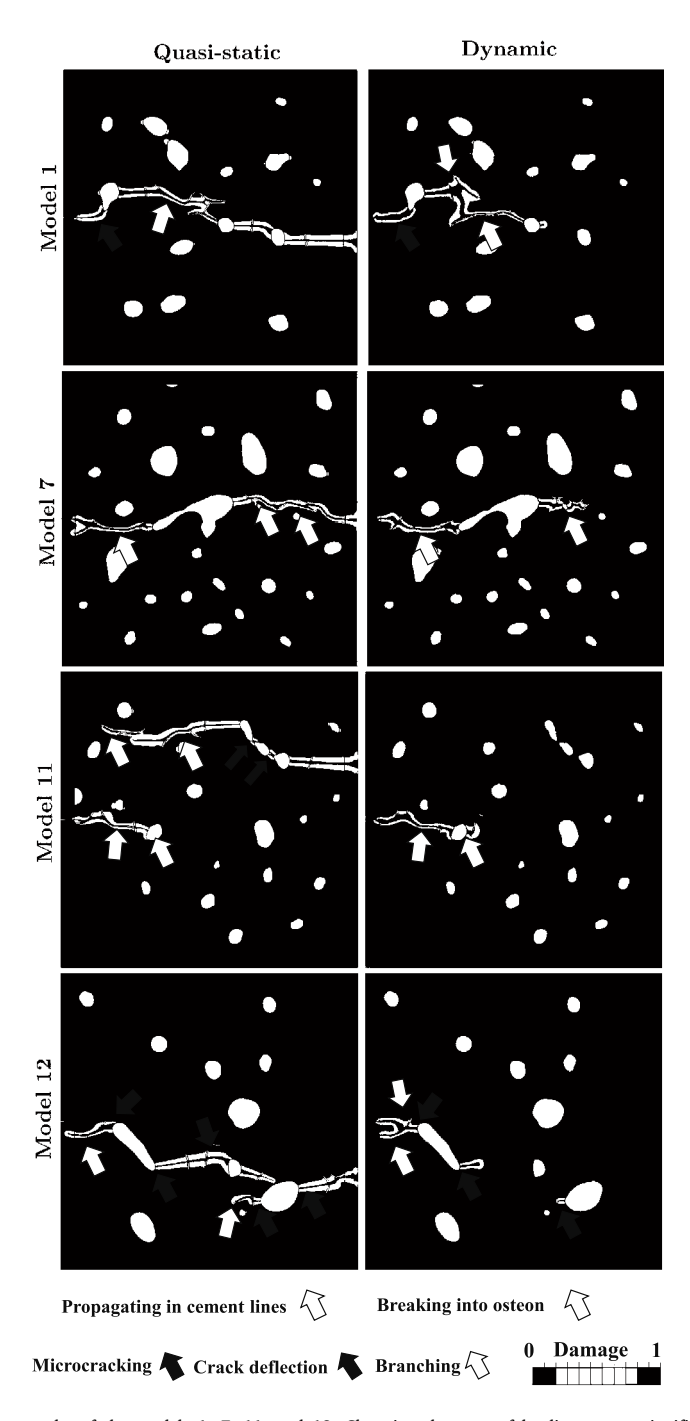


Fig. 7. The quasi-static and dynamic fracture results of the models 1, 7, 11, and 12. Changing the type of loading causes significant differences in crack growth trajectories between the two loading types for each model. The reason for observing more damage in the quasi-static results rather than the dynamic results is due to the time increment. In the quasi-static cases, the models have the whole time for a complete fracture to occur. However, in the dynamic cases, the models are under an instantaneous loading that occurs very quickly.

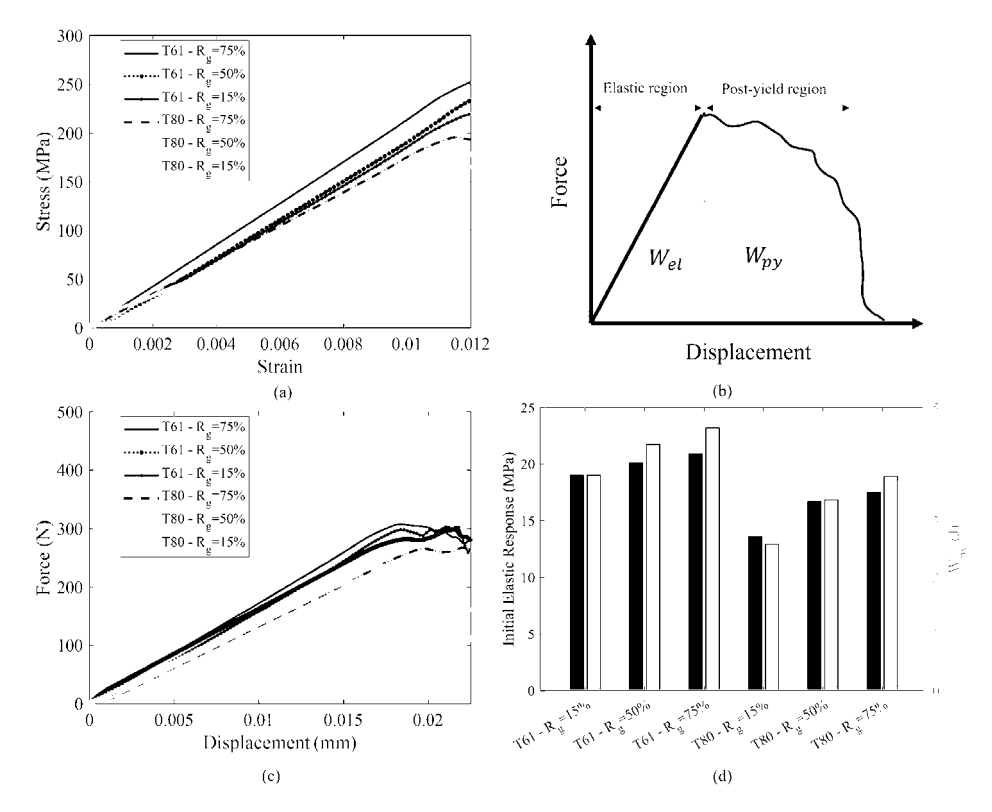


Fig. 8. (a) The stress–strain curves for the initial elastic response of the bones with different ages and different possible mismatches, (b) The elastic energy absorbed  $W_{el}$  (left shaded area) and post-yield energy absorption, and (d) Calculated effective elastic response of bone as well as post-yield energy absorption for different ages and possible material mismatches in the bone. With an increase in age and AGEs level, the effective elastic stiffness of bone decreases as bone becomes more brittle, and the capacity to absorb energy drops accordingly.

of cortical bone with different levels of AGEs cannot be ignored. Moreover, the rate of loading in cortical bone can activate and deactivate the toughening mechanisms and impact crack growth trajectories.

## CRediT authorship contribution statement

**Ebrahim Maghami:** Writing – review & editing, Writing – original draft, Visualization, Software, Methodology, Investigation, Formal analysis. **Amirreza Sadighi:** Writing – review & editing, Visualization, Software, Methodology, Investigation. **Ahmad R. Najafi:** Writing – review & editing, Supervision, Project administration, Methodology, Funding acquisition, Conceptualization.

## **Declaration of competing interest**

The authors declare that they have no known competing financial interests or personal relationships that could have appeared to influence the work reported in this paper.

## Data availability

Data will be made available on request.

## Acknowledgments

The authors acknowledge the high-performance computing resources (Picotte: the Drexel Cluster) and support at Drexel University. We thank Dr. Theresa A. Freeman and the laboratory facilities of Thomas Jefferson University. We are grateful to Timothy O. Josephson and Jason P. Moore for the sectioning, staining, and imaging of bone samples. We thank Dr. Lamya Karim and Taraneh Rezaee at the University of Massachusetts Dartmouth for providing and cutting of the cortical bone samples.

### **Funding**

This study was supported by faculty start-up funding from the Department of Mechanical Engineering and Mechanics at Drexel University. The development of the dynamic fracture framework is also supported by the NSF CAREER Award CMMI-2143422.

## References

Abdel-Wahab, A.A., Maligno, A.R., Silberschmidt, V.V., 2012. Micro-scale modelling of bovine cortical bone fracture: Analysis of crack propagation and microstructure using X-FEM. Comput. Mater. Sci. 52 (1), 128–135.

Augat, P., Schorlemmer, S., 2006. The role of cortical bone and its microstructure in bone strength. Age Ageing 35 (suppl\_2), ii27-ii31.

Bourdin, B., Francfort, G.A., Marigo, J.-J., 2008. The variational approach to fracture. J. Elasticity 91 (1–3), 5–148.

Brown, C.U., Yeni, Y.N., Norman, T.L., 2000. Fracture toughness is dependent on bone location—A study of the femoral neck, femoral shaft, and the tibial shaft. J. Biomed. Mater. Res.: Off. J. Soc. Biomater. Jpn. Soc. Biomater. 49 (3), 380–389.

Budyn, E., Hoc, T., Jonvaux, J., 2008. Fracture strength assessment and aging signs detection in human cortical bone using an X-FEM multiple scale approach. Comput. Mech. 42 (4), 579–591.

Burr, D.B., 2019. Changes in bone matrix properties with aging. Bone 120, 85-93.

Campbell, G.M., Tiwari, S., Hofbauer, C., Picke, A.-K., Rauner, M., Huber, G., Peña, J.A., Damm, T., Barkmann, R., Morlock, M., et al., 2016. Effects of parathyroid hormone on cortical porosity, non-enzymatic glycation and bone tissue mechanics in rats with type 2 diabetes mellitus. Bone 82, 116–121.

Carando, S., Barbos, M.P., Ascenzi, A., Boyde, A., 1989. Orientation of collagen in human tibial and fibular shaft and possible correlation with mechanical properties. Bone 10 (2), 139–142.

Collier, T., Nash, A., Birch, H., De Leeuw, N., 2018. Effect on the mechanical properties of type I collagen of intra-molecular lysine-arginine derived advanced glycation end-product cross-linking. J. Biomech. 67, 55–61.

de Borst, R., Verhoosel, C.V., 2016. Gradient damage vs phase-field approaches for fracture: Similarities and differences. Comput. Methods Appl. Mech. Engrg. 312, 78–94.

Fan, Z., Swadener, J., Rho, J., Roy, M., Pharr, G., 2002. Anisotropic properties of human tibial cortical bone as measured by nanoindentation. J. Orthop. Res. 20 (4), 806–810.

- Fratzl, P., Gupta, H., Paschalis, E., Roschger, P., 2004. Structure and mechanical quality of the collagen-mineral nano-composite in bone. J. Mater. Chem. 14 (14), 2115-2123
- Gauthier, R., Follet, H., Olivier, C., Mitton, D., Peyrin, F., 2019. 3D analysis of the osteonal and interstitial tissue in human radii cortical bone. Bone 127, 526–536.
- Giner, E., Belda, R., Arango, C., Vercher-Martínez, A., Tarancón, J.E., Fuenmayor, F.J., 2017. Calculation of the critical energy release rate gc of the cement line in cortical bone combining experimental tests and finite element models. Eng. Fract. Mech. 184. 168–182.
- Gustafsson, A., Khayyeri, H., Wallin, M., Isaksson, H., 2019. An interface damage model that captures crack propagation at the microscale in cortical bone using XFEM. J. Mech. Behav. Biomed. Mater. 90, 556–565.
- Hansen, U., Zioupos, P., Simpson, R., Currey, J.D., Hynd, D., 2008. The effect of strain rate on the mechanical properties of human cortical bone. J. Biomech. Eng. 130 (1).
- Hofacker, M., Miehe, C., 2012. Continuum phase field modeling of dynamic fracture: variational principles and staggered FE implementation. Int. J. Fracture 178 (1), 113–129
- Hofacker, M., Miehe, C., 2013. A phase field model of dynamic fracture: Robust field updates for the analysis of complex crack patterns. Internat. J. Numer. Methods Engrg. 93 (3), 276–301.
- Jia, S., Gong, H., Cen, H., Shi, P., Zhang, R., Li, Z., Bi, X., 2021. Influence of non-enzymatic glycation on the mechanical properties of cortical bone. J. Mech. Behav. Biomed. Mater. 119, 104553.
- Josephson, T.O., Moore, J.P., Maghami, E., Freeman, T.A., Najafi, A.R., 2022. Computational study of the mechanical influence of lacunae and perilacunar zones in cortical bone microcracking. J. Mech. Behav. Biomed. Mater. 126, 105029.
- Karim, L., Bouxsein, M.L., 2016. Effect of type 2 diabetes-related non-enzymatic glycation on bone biomechanical properties. Bone 82, 21–27.
- Karim, L., Rezaee, T., Vaidya, R., 2019. The effect of type 2 diabetes on bone biomechanics. Curr. Osteoporos. Rep. 17 (5), 291–300.
- Kirchner, H., 2006. Ductility and brittleness of bone. Int. J. Fracture 139 (3), 509–516.
   Kulin, R.M., Jiang, F., Vecchio, K.S., 2011. Loading rate effects on the R-curve behavior of cortical bone. Acta Biomater. 7 (2), 724–732.
- Li, S., Abdel-Wahab, A., Demirci, E., Silberschmidt, V.V., 2014. Fracture process in cortical bone: X-FEM analysis of microstructured models. In: Fracture Phenomena in Nature and Technology. Springer, pp. 43–55.
- Liu, G., Li, Q., Msekh, M.A., Zuo, Z., 2016. Abaqus implementation of monolithic and staggered schemes for quasi-static and dynamic fracture phase-field model. Comput. Mater. Sci. 121, 35–47.
- Maghami, E., Josephson, T.O., Moore, J.P., Rezaee, T., Freeman, T.A., Karim, L., Najafi, A.R., 2021a. Fracture behavior of human cortical bone: Role of advanced glycation end-products and microstructural features. J. Biomech. 125, 110600.
- Maghami, E., Moore, J.P., Josephson, T.O., Najafi, A.R., 2022. Damage analysis of human cortical bone under compressive and tensile loadings. Comput. Methods Biomech. Biomed. Eng. 25 (3), 342–357.
- Maghami, E., Pejman, R., Najafi, A.R., 2021b. Fracture micromechanics of human dentin: A microscale numerical model. J. Mech. Behav. Biomed. Mater. 114, 104171.
- Mandal, T.K., Nguyen, V.P., Wu, J.-Y., 2019. Length scale and mesh bias sensitivity of phase-field models for brittle and cohesive fracture. Eng. Fract. Mech. 217, 106532.
- Merlo, K., Aaronson, J., Vaidya, R., Rezaee, T., Chalivendra, V., Karim, L., 2020. In vitro-induced high sugar environments deteriorate human cortical bone elastic modulus and fracture toughness. J. Orthop. Res. 38 (5), 972–983.
- Miehe, C., Hofacker, M., Welschinger, F., 2010. A phase field model for rate-independent crack propagation: Robust algorithmic implementation based on operator splits. Comput. Methods Appl. Mech. Engrg. 199 (45–48), 2765–2778.
- Mischinski, S., Ural, A., 2013. Interaction of microstructure and microcrack growth in cortical bone: A finite element study. Comput. Methods Biomech. Biomed. Eng. 16 (1), 81–94.
- Molnár, G., Gravouil, A., 2017. 2D and 3D abaqus implementation of a robust staggered phase-field solution for modeling brittle fracture. Finite Elem. Anal. Des. 130, 27–38.
- Molnar, G., Gravouil, A., Seghir, R., Réthoré, J., 2020. An open-source abaqus implementation of the phase-field method to study the effect of plasticity on the instantaneous fracture toughness in dynamic crack propagation. Comput. Methods Appl. Mech. Engrg. 365, 113004.
- Msekh, M.A., Cuong, N., Zi, G., Areias, P., Zhuang, X., Rabczuk, T., 2018. Fracture properties prediction of clay/epoxy nanocomposites with interphase zones using a phase field model. Eng. Fract. Mech. 188, 287–299.

- Najafi, A.R., Saffar, K.P.A., Arshi, A.R., Mallakin, E., Katouzian, H.R., Eslami, M.R., Moeinzadeh, M.H., 2011. Propagation of microcracks in bovine osteonal cortical bone. Akademeia 1 (1), pp. 1923-1504.
- Nguyen, C., Peetz, D., Elbanna, A.E., Carlson, J.M., 2019. Characterization of fracture in topology-optimized bioinspired networks. Phys. Rev. E 100 (4), 042402.
- Nguyen, L., Stoter, S., Baum, T., Kirschke, J., Ruess, M., Yosibash, Z., Schillinger, D., 2017. Phase-field boundary conditions for the voxel finite cell method: Surface-free stress analysis of CT-based bone structures. Int. J. Numer. Methods Biomed. Eng. 33 (12), e2880.
- Nguyen, T.T., Yvonnet, J., Zhu, Q.-Z., Bornert, M., Chateau, C., 2015. A phase field method to simulate crack nucleation and propagation in strongly heterogeneous materials from direct imaging of their microstructure. Eng. Fract. Mech. 139, 18–39.
- Nyman, J.S., 2013. Effect of diabetes on the fracture resistance of bone. Clin. Rev. Bone Miner. Metabol. 11 (1), 38–48.
- Nyman, J.S., Roy, A., Tyler, J.H., Acuna, R.L., Gayle, H.J., Wang, X., 2007. Age-related factors affecting the postyield energy dissipation of human cortical bone. J. Orthop. Res. 25 (5), 646–655.
- Phelps, J., Hubbard, G., Wang, X., Agrawal, C., 2000. Microstructural heterogeneity and the fracture toughness of bone. J. Biomed. Mater. Res. 51 (4), 735–741.
- Pinto, D.C., Pace, E.D., 2015. A silver-stain modification of standard histological slide preparation for use in anthropology analyses. J. Forensic Sci. 60 (2), 391–398.
- Poundarik, A.A., Wu, P.-C., Evis, Z., Sroga, G.E., Ural, A., Rubin, M., Vashishth, D., 2015. A direct role of collagen glycation in bone fracture. J. Mech. Behav. Biomed. Mater. 52, 120–130.
- Rho, J.-Y., Kuhn-Spearing, L., Zioupos, P., 1998. Mechanical properties and the hierarchical structure of bone. Med. Eng. Phys. 20 (2), 92–102.
- Saffar, K.P., Najafi, A.R., Moeinzadeh, M.H., Sudak, L.J., 2013. A finite element study of crack behavior for carbon nanotube reinforced bone cement. World J. Mech. 3 (5A), 13–21.
- Saito, M., Mori, S., Mashiba, T., Komatsubara, S., Marumo, K., 2008. Collagen maturity, glycation induced-pentosidine, and mineralization are increased following 3-year treatment with incadronate in dogs. Osteoporos. Int. 19 (9), 1343–1354.
- Shannahan, L., Weerasooriya, T., Gunnarsson, A., Sanborn, B., Lamberson, L., 2015.
  Rate-dependent fracture modes in human femoral cortical bone. Int. J. Fract. 194
  (2), 81–92.
- Tang, S., Allen, M.R., Phipps, R., Burr, D.B., Vashishth, D., 2009. Changes in non-enzymatic glycation and its association with altered mechanical properties following 1-year treatment with risedronate or alendronate. Osteoporos. Int. 20 (6), 887–894.
- Tang, S., Vashishth, D., 2010. Non-enzymatic glycation alters microdamage formation in human cancellous bone. Bone 46 (1), 148–154.
- Tang, S., Vashishth, D., 2011. The relative contributions of non-enzymatic glycation and cortical porosity on the fracture toughness of aging bone. J. Biomech. 44 (2), 330–336.
- Tomar, V., 2008. Modeling of dynamic fracture and damage in two-dimensional trabecular bone microstructures using the cohesive finite element method. J. Biomech. Eng. 130 (2), 021021.
- Ural, A., Zioupos, P., Buchanan, D., Vashishth, D., 2011. The effect of strain rate on fracture toughness of human cortical bone: A finite element study. J. Mech. Behav. Biomed. Mater. 4 (7), 1021–1032.
- Vashishth, D., 2009. Advanced glycation end-products and bone fractures. Ibms Bonekey 6 (8), 268.
- Verhoosel, C.V., de Borst, R., 2013. A phase-field model for cohesive fracture. Int. J. Numer. Methods Eng. 96 (1), 43–62.
- Wu, C., Fang, J., Zhang, Z., Entezari, A., Sun, G., Swain, M.V., Li, Q., 2020. Fracture modeling of brittle biomaterials by the phase-field method. Eng. Fract. Mech. 224, 106752.
- Wu, J.-Y., Nguyen, V.P., Nguyen, C.T., Sutula, D., Bordas, S., Sinaie, S., 2018. Phase field modeling of fracture. In: Advances in Applied Mechancis: Multi-Scale Theory and Computation, vol. 52.
- Zhang, X., Vignes, C., Sloan, S.W., Sheng, D., 2017. Numerical evaluation of the phase-field model for brittle fracture with emphasis on the length scale. Comput. Mech. 59, 737–752.
- Zimmermann, E.A., Gludovatz, B., Schaible, E., Busse, B., Ritchie, R.O., 2014. Fracture resistance of human cortical bone across multiple length-scales at physiological strain rates. Biomaterials 35 (21), 5472–5481.
- Zioupos, P., Hansen, U., Currey, J.D., 2008. Microcracking damage and the fracture process in relation to strain rate in human cortical bone tensile failure. J. Biomech. 41 (14), 2932–2939.